JOURNAL OF APPLIED POLYMER SCIENCE VOL. 20 169–191 (1976)

Studies on Melt Spinning. VI. Simulation of Draw Resonance Using Newtonian and Power Law Viscosities

HIDEAKI ISHIHARA, *Katata Research Institute, Toyobo Co., Ltd., Ohtsushi Shigaken 520-02, Japan* and SUSUMU KASE, *Technical Exports and Licensing Division, Toyobo Co., Ltd., Kitaku Dojima, Osaka 530, Japan*

Synopsis

Draw resonance, a periodic variation of spin line diameter in unstable melt spinning, was measured for its wave form under 34 different spinning conditions for PET and PP. In an attempt to simulate the measured wave form, the equations of continuity and momentum for the isothermal melt spinning of power law fluids were solved for their limit cycle solutions expressed in the time variations in the cross-sectional area at the take-up. Power law exponent p and draw down ratio ψ_w uniquely define the solution. Theoretical curves were superposed on the experimental amplitude-versus-ψ_w diagram and oscillation period-versus-ψ_w diagram to assign p value to each experimental point. Excellent agreement between theory and experiment was obtained with PET in that p values were nearly independent of ψ_w and of the diagram used in the determination of the p value, amplitude diagram, or oscillation period diagram. Motion pictures (16 mm) of the side profiles of the pulsing spinline showed good agreement with the theoretical side profiles constructed from the corresponding limit cycle solution. It was proposed that the stability of melt spinning has no direct equivalence to the spinnability of fluids.

INTRODUCTION

When the process of melt spinning becomes unstable, standing wave-type variations in the thickness of the filament taken up develop. This pulsing phenomenon has been called "draw resonance" since Miller[1] first used the term in his early paper.

Subsequently, several researchers[2–8] made attempts to analyze draw resonance by means of perturbation studies of the equations of momentum, continuity, and energy set up for the conditions of melt spinning. Their studies established to a reasonable certainty that draw resonance is the result of an instability in the classical sense of the process of melt spinning and that (i) cooling of the filament in the air gap plays a predominant role in stabilizing the conventional industrial melt spinning[9]; (ii) shear thickening of the polymer, that is, increasing the exponent p in the power law model, tends to stabilize the spinning[6]; and (iii) the isothermal spinning of Newtonian fluids is unstable[2,4] when the draw-don ratio of spinning is more than 20.

Kase[2,9] compared theoretical results with experiments in PP film casting and found that the two agreed very well in oscillation period.

While these perturbation studies were successful in predicting the oscillation period and approximate conditions of neutral stability, they failed to predict the exact wave form of draw resonance, notably the amplitude, since some information is lost when the equations are linearized.

To overcome this drawback, the authors[10] solved the equations of continuity and momentum for isothermal spinning directly without recourse to perturbation. The solutions obtained were limit cycles, standing waves of constant amplitude and period, in agreement with the general wave form of draw resonance. Similar results were obtained by Fisher and Denn[11] by means of a different approach.

The present study, still concerning draw resonance in isothermal spinning, extends and supplements the previous study[10] in the following respects: (i) the polymer viscosity model was extended from the Newtonian to include the power law fluid, (ii) additional experimental observations of isothermal draw resonance were carried out with improved precision in an effort to obtain a better verification of the limit cycle solution; and (iii) motion pictures (16 mm) were taken of the side profiles of the pulsing spinline in draw resonance, and the pictures were compared with the theoretical side profiles derived from the limit cycle solution to demonstrate the validity of the solution and to show the wave-like nature of draw resonance.

THEORETICAL

Power Law Fluids

Using the assumptions made in a previous paper,[12] the governing equations for the isothermal spinning of power law fluids are

$$\frac{\partial v}{\partial x} = \frac{F}{A\beta} \tag{1}$$

$$\frac{\partial A}{\partial \tau} + \frac{\partial (Av)}{\partial x} = 0 \tag{2}$$

$$\beta = \beta_0 (\partial v/\partial x)^{p-1} \tag{3}$$

where x is the axial coordinate, in cm, measured downstream from where the maximum filament diameter occurs due to die swell; τ is time, in sec; A is cross-sectional area, in cm^2; v is axial velocity, in cm/sec; F is filament tension, in gram weight; and β_0 and p are material constants.

Boundary conditions are identical to those used in the analysis[10] of isothermal Newtonian liquids:

(i) Fixed velocity v_{00} and filament thickness A_{00} at the point where the filament diameter is maximum due to die swell. Since this point is very close to the die exit, we call it hereafter simply die exit and denote it by a subscript 00.

(ii) Fixed take-up velocity v_w, where subscript w denotes the values at the take-up point.

Equations (1) and (2) are converted into a nondimensional form by defining the following variables.

$$\zeta = x/x_w \qquad \text{nondimensional distance} \tag{4}$$

$$\tau^* = \tau v_{00}/x_w \qquad \text{nondimensional time} \tag{5}$$

$$\lambda = A/A_{00} \qquad \text{nondimensional filament thickness} \tag{6}$$

$$\psi = v/v_{00} \qquad \text{nondimensional axial velocity} \tag{7}$$

$$\xi = \frac{F}{A_{00}\beta_0}\left(\frac{x_w}{v_{00}}\right)^p \qquad \text{nondimensional tension} \tag{8}$$

Except for ξ, these nondimensional variables have the same definitions as those used in the analysis[10] of Newtonian liquids. Equations (1) and (2) now become

$$\frac{\partial \psi}{\partial \zeta} = \left(\frac{\xi}{\lambda}\right)^q \tag{9}$$

$$\frac{\partial \lambda}{\partial \tau^*} + \frac{\partial}{\partial \zeta}(\lambda\psi) = 0 \tag{10}$$

where

$$q = 1/p \tag{11}$$

Steady-state solutions of eqs. (9) and (10), denoted by subscript 0, are

$$\psi_0 = \{(\psi_w{}^{1-q} - 1)\zeta + 1\}^{1/(1-q)} \tag{12}$$

$$\lambda_0 = \{(\psi_w{}^{1-q} - 1)\zeta + 1\}^{-1/(1-q)} \tag{13}$$

where ψ_w is the draw-down ratio of melt spinning.

We further replace dependent variables ψ and λ with ratios V and W defined below in the same manner as in the case[10] of Newtonian fluids:

$$\psi = V\psi_0 \tag{14}$$

$$\lambda = W\psi_0. \tag{15}$$

Dimensionless distance ζ, too, is replaced with dimensionless residence time ζ^* defined below:

$$\zeta^* = \int_0^\zeta \lambda_0 d\zeta = \frac{q-1}{q(\psi_w{}^{1-q} - 1)}[\{(\psi_w{}^{1-q} - 1)\zeta + 1\}^{q/(q-1)} - 1]. \tag{16}$$

The value of ζ^* at the take-up point ($\zeta = 1$) is

$$\zeta_w{}^* = \frac{(q-1)(\psi_w{}^{-q} - 1)}{q(\psi_w{}^{1-q} - 1)}. \tag{17}$$

Using eqs. (12) through (16), eqs. (9) and (10) become

$$\frac{\partial V}{\partial \zeta^*} - \frac{V}{q(\zeta^* + \omega)} = \left(\frac{\xi}{W}\right)^q \frac{\omega}{\zeta^* + \omega} \tag{18}$$

$$\frac{\partial W}{\partial \tau^*} + \frac{\partial}{\partial \zeta^*}(VW) = 0 \tag{19}$$

where

$$\omega = \frac{q-1}{q\left(\psi\dfrac{1-q}{w}-1\right)}. \tag{20}$$

Boundary conditions (i) and (ii) are rewritten in terms of dimensionless variables as (i) $V = W = 1$, at $\zeta^* = 0$; and (ii) $V = \text{const}$ (= 1.1 in the present study), at $\zeta^* = \zeta_w^*$.

Since p and ψ_w are the only parameters contained in eqs. (18) and (19) and the boundary conditions above, solutions are uniquely defined by these two parameters. Dimensionless spinning tension ξ is an extra dependent variable whose values are decided to satisfy the boundary condition (ii) above.

It is noteworthy that solution in $V(\zeta^*, \tau^*)$ or $W(\zeta^*, \tau^*)$ is independent of such physical parameters as x_w, v_{00}, A_{00}, or β_0.

Since analytical solution is not available on eqs. (18) and (19), numerical solution becomes mandatory. For this purpose, eqs. (18) and (19) are converted into the difference eqs. (21) and (22) using a simple backward difference scheme as in a previous paper[10]:

$$V_{i+1,j+1} = F_3 + F_2(W_{i+1,j+1})^{-q} \tag{21}$$

$$W_{i+1,j+1} = \frac{F_1}{1 + V_{i+1,j+1}} \tag{22}$$

where

$$F_1 = W_{i+1,j} + V_{i,j+1}W_{i,j+1} \tag{23}$$

$$F_2 = \frac{\omega\xi^q}{(\zeta^* + \omega)/\Delta - 1/q} \tag{24}$$

$$F_3 = \frac{(\zeta^* + \omega)/\Delta V_{i,j+1}}{(\zeta^* + \omega)/\Delta - 1/q} \tag{25}$$

$$\Delta = \Delta\zeta^* = \Delta\tau^* = \zeta_w^*/N. \tag{26}$$

There is a difficulty involved in the above numerical scheme in that eqs. (21) and (22) cannot be solved for $V_{i+1,j+1}$ and $W_{i+1,j+1}$ explicitly. Use of formal iterative process in solving eqs. (21) and (22) on each (i,j) mesh point, on the other hand, is prohibitive with respect to computer time. To overcome this difficulty, eq. (21) is replaced by an approximate formula

$$V_{i+1,j+1} = F_3 + F_2\left(\frac{F_1}{1 + V_{i,j+1}}\right)^{-q} \tag{27}$$

where the value in parenthesis is a slight modification of the right hand side of eq. (22). Errors incurred by this approximation is expected to diminish with increasing number N of differencing increments. Besides, the error can be evaluated by setting the value of q close to unity and comparing the solution thus obtained with that of corresponding Newtonian equations[10] which involve no approximation of this kind. It should be noted that the Newtonian case of $p = q = 1$ cannot be handled by eq. (18) since ω becomes infinitely large as q approaches unity. In this case, eq. (28) developed in the previous study[10] has to be used in place of eq. (18):

$$\frac{\partial V}{\partial \zeta^*} + \frac{\log \psi_w}{1 - (\log \psi_w)\zeta^*} V = \frac{\xi}{W} \frac{1}{1 - (\log \psi_w)\zeta^*}. \tag{28}$$

The finite difference equation derived from eq. (28) is

$$V_{i+1,j+1} = (1 + F_1F_3)/F_1F_2 - 1) \tag{29}$$

where

$$F_1 = W_{i+1,j} + V_{i,j+1}W_{i,j+1} \tag{30}$$

$$F_2 = (1 - \zeta^* \log \psi_w)/(\xi\Delta) + (\log \psi_w)/\xi \tag{31}$$

$$F_3 = (1 - \zeta^* \log \psi_w)V_{i,j+1}/(\xi\Delta). \tag{32}$$

As discussed in a previous paper,[10] the wave form of limit cycle is independent of initial conditions; the solution expressed in $W_{i_w,j}$ settles to a standing wave of fixed amplitude and period after the decay of the initial transient. For this reason, any initial values can be given to $W_{i,1}$ with the restriction that they are positive and $W_{1,1}$ is equal to unity. With some experience and skill, it becomes possible to set the $W_{i,1}$ values in such a way to make the initial transient short saving the computer time.

In principle, the initial $V_{i,1}$ values have to be derived from the given $W_{i,1}$ values using eq. (21) in an iterative process to satisfy the boundary condition (ii). The initial $V_{i,1}$ values, however, turn out to be irrelevant in subsequent computations and need not be computed since the right-hand sides of eqs. (21) and (22) do not contain either $V_{i,j}$ or $V_{i+1,j}$.

The numerical solution of eqs. (21) and (22) proceeds in the following manner: (a) j is set to 1; (b) initial values are given to $W_{i,1}$; (c) an arbitrary value is given to ξ; (d) $V_{1,j}$ through $V_{i_w,j}$ and $W_{1,j}$ through $W_{i_w,j}$ are computed successively using the boundary condition (i) and eqs. (21) and (22); (e) ξ is changed using Newton's formula, and c and d above are repeated until the boundary condition (ii) is satisfied within a predetermined tolerance; (f) j is increased by 1, and steps c through f above are repeated until the solution settles to a limit cycle.

Computation for one spinning condition took about 5 min on an IBM-370-158 machine when N was equal to 100 and the endpoint of computation was j = 5000. Computation time was found to be roughly in proportion to the number of mesh points used in the computation. The number is equal to N times the number of steps in j computed. As eq. (26) shows, independent variables ζ^* and τ^* share a common difference increment Δ. For this reason, the $j = N$ point on the j scale always correspond to $\tau^* = \zeta_w^*$, the nondimensional residence time of the polymer in the steady-state spinning.

Limit Cycle Solutions for the Power Law Model

Difference eqs. (21) and (22) were solved numerically to satisfy the boundary conditions (i) and (ii) as discussed in the previous section for various values of power law exponent p and log draw-down ratio log ψ_w. Except for the effects of the number N of difference increments, p and ψ_w are the only parameters that affect the solutions. Both limit cycle solutions and stable solutions as listed in Table I were obtained. Solution characteristics shown

TABLE I
Limit Cycle Solutions for Power Law Model[a]

No.	log ψ_w	p	τ_c*	W_{max}	W_{min}	ξ_{max}/ξ_0	N
1	2.095	0.60		2.58	0.229	1.80	100
2	2.095	0.75		NS			100
3	2.095	0.80		S			100
4	2.095	1.00		S			100
5	2.595	0.90		NS			100
6	2.595	1.00		S			100
7	3.095	0.75	0.7034	8.21	0.036	3.88	100
8	3.095	0.90	0.5590	4.29	0.137	2.70	100
9	3.095	1.00		NS			100
10	3.295	1.00	0.4600	2.36	0.32	1.88	100
11	3.295	1.05	0.4152	1.12	0.711	1.23	100
12	3.595	0.95	0.5679	8.40	0.051	4.42	100
13	3.595	1.00	0.5019	5.88	0.100	3.5	100
14	3.595	1.05	0.3409	4.64	0.134	3.28	100
15	3.595	1.10	0.4029	2.50	0.303	2.03	100
16	3.595	1.15	0.3617	1.21	0.69	1.26	100
17	3.595	1.20	0.3311	0.925	0.86	1.08	100
18	3.595	1.30		S			
19	3.895	0.95	0.5951	12.63	0.025	6.34	100
20	3.895	1.00	0.5348	9.5	0.048		100
21	3.895	1.05	0.4104	8.45	0.057	4.59	100
22	3.895	1.30		S			100
23	4.095	0.95	0.6114	15.91	0.016	7.53	100
24	4.095	1.00	0.5467	12.7	0.033	6.1	100
25	4.095	1.05	0.5144	11.41	0.036	6.66	100
26	4.095	1.10	0.4681	9.02	0.055	5.60	100
27	4.095	1.20	0.3546	3.95	0.176	3.17	100
28	4.095	1.30	0.2858	1.07	0.793	1.15	100
29	4.335	1.00	0.5568	16.7	0.022	7.5	100
30	4.335	1.35	0.2583	1.19	0.676	1.30	100
31	4.335	1.45		S			100
32	4.445	1.10	0.4944	15.0	0.023	7.7	100
33	4.445	1.20	0.3963	9.1	0.057	5.9	100
34	4.445	1.30	0.3048	4.2	0.183	3.5	100
35	4.445	1.40	0.2301		0.855	1.12	100
36	4.445	1.50		S			100
37	4.595	1.45	0.2196	1.06	0.811	1.16	100
38	4.595	1.50		S			100
39	3.295	1.00	0.5292	5.49	0.102	3.23	400
40	3.595	1.00	0.5887	10.75	0.0399	5.00	400
41	3.595	1.10	0.4645	5.66	0.104	3.49	400
42	3.895	1.00	0.6287	17.11	0.0214	6.95	400
43	3.895	1.20	0.4000	5.57	0.111	3.83	400
44	4.095	1.00	0.6463	22.11	0.0155	8.41	400
45	4.095	1.10	0.5648	17.27	0.022	7.74	400
46	4.095	1.20	0.4507	10.38	0.048	6.05	400
47	4.095	1.25	0.3709	5.93	0.110	4.07	400
48	4.445	1.20	0.4961	20.47	0.020	10.05	400

[a] log ψ_w = log draw down ratio; p = power law exponent; τ_c* = dimensionless oscillation period, W_{max}, W_{min} = peak and valley values of dimensionless cross-section area at take-up; ξ_{max}, ξ_{min} = peak and steady-state values of dimensionless spinning tension. Stable and near stable solutions are marked with S and NS on the W_{max} column.

in Table I are p, log ψ_w, nondimensional oscillation period τ_c^*, peak W_{max} and valley W_{min} values of $W_{i_w,j}$, and the ratio ξ_{max}/ξ_0 of peak spinning tension to average spinning tension. Stable solutions are marked with the letter S.

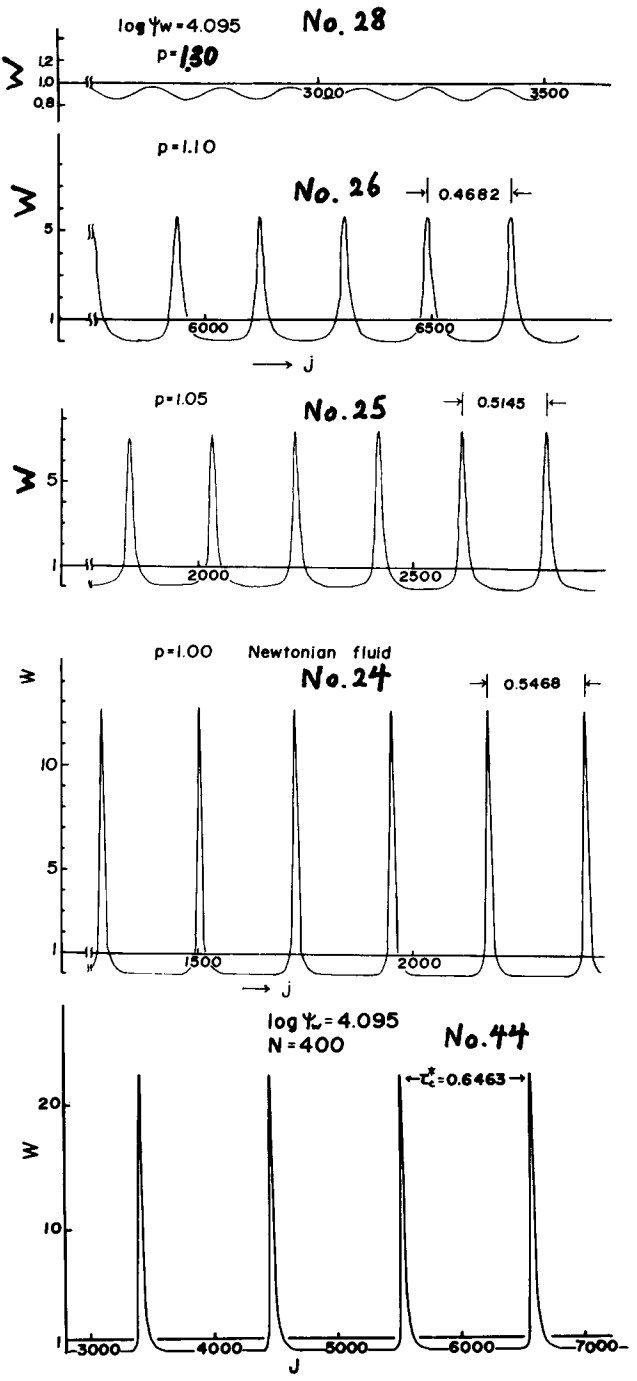

Fig. 1. Limit cycle solutions with the power law model expressed as time variations in dimensionless cross-sectional area W at the take-up point.

Some of the limit cycle solutions listed in Table I are shown in Figure 1 as $W_{i_w,j}$-versus-j curves to demonstrate the general wave form. In Figure 1, $j = N$ correspond to the steady-state residence time of the melt-spinning system. Shown enlarged in Figure 2 is a wave peak of one of the limit cycle solutions computed at $N = 400$ to demonstrate the peculiar skew in the wave form.

To economize computer time, solutions 1 through 38 in Table I were computed setting N equal to 100. This gave a quick view of the general trend of the solutions. These 38 solutions were then summarized graphically by constructing the contours of constant W_{max}, W_{max}/W_{min}, and τ_c* on the p-ver-

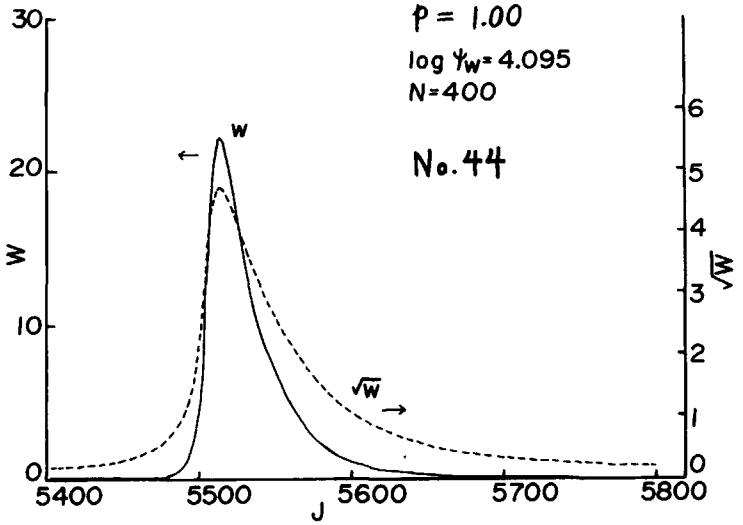

Fig. 2. Skewed wave form of the limit cycle solution.

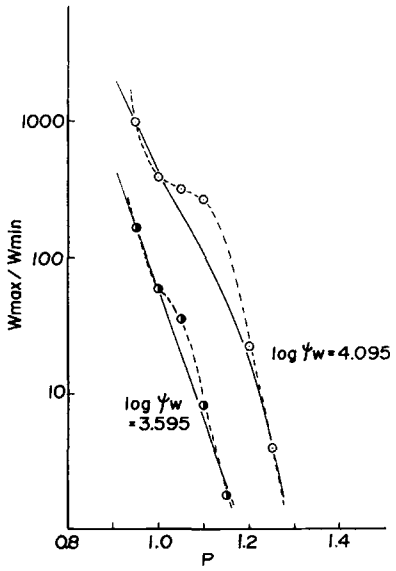

Fig. 3. Inflections on the W_{max}/W_{min} vs. p curves due to the use of the approximate formula eq. (27).

sus-log ψ_w plane. In constructing these contours, it was noted that the W_{max}/W_{min} values plotted against p showed a peculiar inflection near the Newtonian value of $p = 1$, as shown in Figure 3. The inflection was estimated to be caused by the use of the approximate formula, eq. (27), in place of the exact formula, eq. (22). The plotted points in Figure 3 were, therefore, smoothed out by the solid curves which pass through the Newtonian points ($p = 1$) derived without approximation from eq. (29).

The number N of differencing increments of 100 was felt not high enough to obtain a reasonable accuracy on the computed values of W_{max}, W_{min}, and τ^*. To test the effect of N on the solution, computations were carried out for the Newtonian case of $p = 1$ and $\log \psi_w = 4.095$ using four different N values, 100, 200, 300, and 400. The W-versus-j curves for $N = 100$ and $N = 300$ differed considerably, as Figure 4 shows. The peak value W_{max} of nondimensional cross-sectional area at the take-up, when plotted against N as shown in Figure 5, approached asymptotically a fixed value which presumably is the exact solution of eqs. (18) and (19). As Figure 5 clearly shows, N has to be at least 400 for a reasonable accuracy of W_{max}.

On account of the above findings, additional solutions 39 through 48 in Table I were computed under $N = 400$, although computer time increased by a factor of about 10 over that for $N = 100$. The solutions for $N = 400$ thus obtained were compared with those for $N = 100$ on the p-versus-log ψ_w plane with the following findings:

(a) Increasing the value of N from 100 to 400 affected the neutral stability curve very little (contour of $W_{max} = 1$).

(b) The same increase in N considerably increased the values of W_{max}, W_{min}, and τ^*, as Figures 4 and 5 show. However, the ratios of increase of

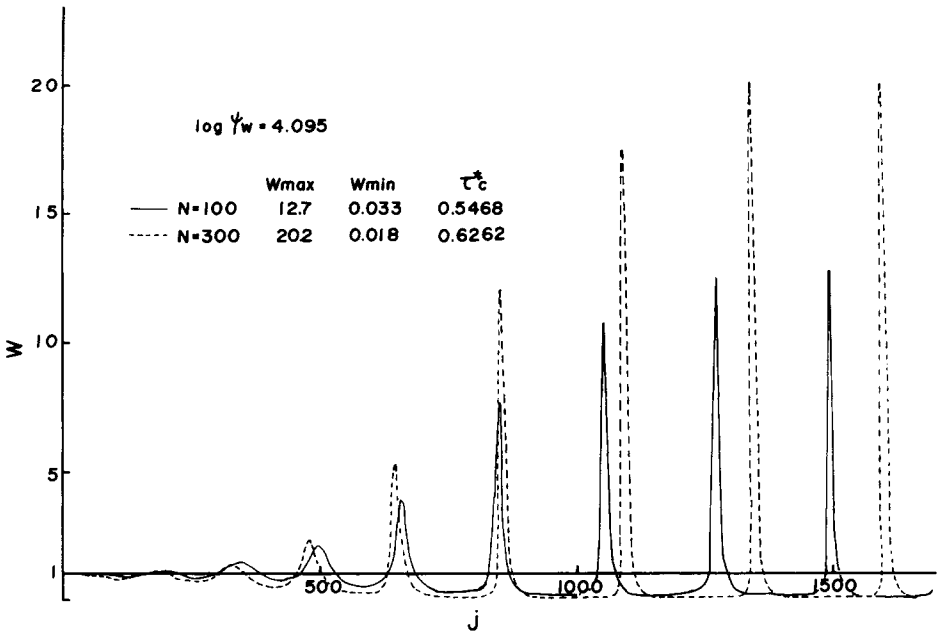

Fig. 4. Influence of the number N of differencing increments on the wave form of the limit cycle solution.

W_{max} and W_{min} remained fairly constant over the region in the p-versus-log ψ_w plane covered by the present study, and the increases in τ^* were likewise consistent and predictable, as Figure 6 suggests.

Taking these findings into consideration, the contours on the p-versus-log $\psi_w{}^*$ plane were modified to make them accurate and compatible with solutions 39 through 48 ($N = 400$). The modified contours of W_{max}, W_{max}/W_{min}, and τ^* are shown in Figures 7 and 8.

The following discussion may be made concerning the above limit cycle solutions:

(i) Changes in p value away from the Newtonian value of 1 in either direction brought changes in amplitude and period, but no marked change in the general nature of wave form (Fig. 1).

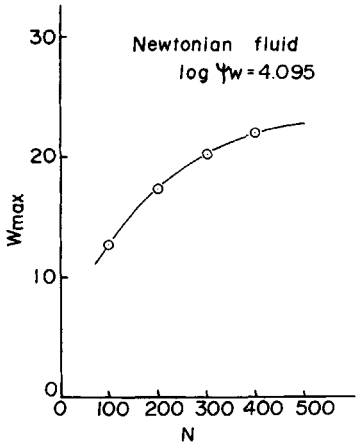

Fig. 5. Asymptotic convergence of W_{max} with increasing N.

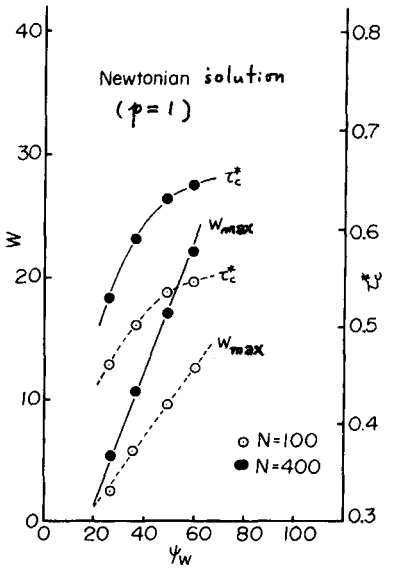

Fig. 6. The systematic and nearly predictable changes in the values of W_{max} and $\tau_c{}^*$ with increasing N.

(ii) The neutral stability curve ($W_{max} = 1$) approximately is a straight line on the p-versus-log ψ_w* plane and is in general agreement with the curve given by Shah and Pearson[6] (Figs. 7 and 8).

(iii) Contours of constant W_{max} and constant W_{max}/W_{min} are approximately straight lines parallel to the neutral stability line. That is to say, the limit cycle solutions on any one of such contours share common W_{max} and W_{min} values. The gradient of these contours is approximately

$$\frac{\Delta p}{\Delta (\log \psi_w)} = -0.29; \tag{33}$$

As far as W_{max} and W_{min} are concerned, therefore, a change in log ψ_w by 1 unit is equivalent to a change in p by -0.29 units (Figs. 7 and 8).

(iv) Contours of constant nondimensional period τ_c* may be expressed approximately as a group of straight lines, as shown in Figure 7. The τ_c* contours, however, are not parallel to each other or to the neutral stability line (Figs. 7 and 8).

(v) Shear thinning liquids ($p < 1$) reaches neutral stability at a draw-down ratio less than the Newtonian value of 20 (Figs. 7 and 8).

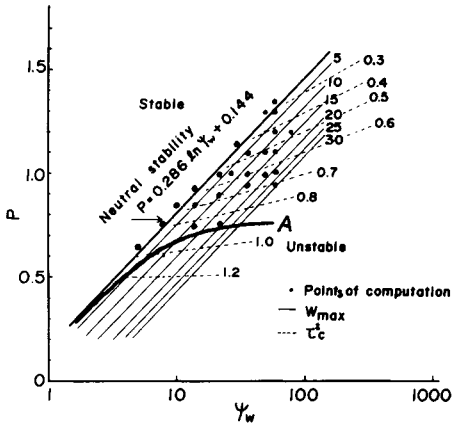

Fig. 7. Contours of constant W_{max} and τ_c* on the p-vs.-log ψ_w plane.

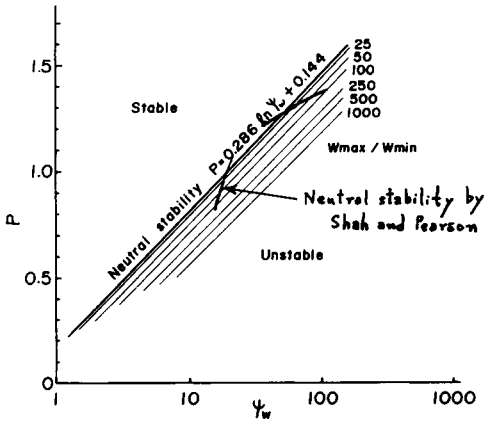

Fig. 8. Contours of constant W_{max}/W_{min} on the p-vs.-log ψ_w plane.

TABLE II
Draw Resonance Experiments[a]

Spinning conditions								Experimental results				
Polymer type and run no.	G, (g/min)	t_{oo}, C	x_w, cm	ψ_w	log ψ_w	v_w, m/min	d_0, μ	d_{max}, μ	d_{min}, μ	L_c, cm	W_{max}	W_{max}/W_{min}
PET-A-1	5.9	280	10	48.6	3.88	190	172	284.0	110.0	160	2.73	6.67
2	5.9	280	5	48.6	3.88	190	172	485.5	55.5	106	7.97	76.5
3	5.9	280	2	48.6	3.88	190	172	436.1	61.0	52	6.43	51.1
4	5.9	280	1	48.6	3.88	190	172	324.0	110.0	23	3.55	8.68
5	5.9	280	0.5	48.6	3.88	190	172	198.9	156.0	18	1.34	1.68
6	5.9	280	2	35.8	3.58	140	200	426.0	97.0	33	4.53	19.3
7	5.9	280	2	79.8	4.38	312	134	438.8	38.0	85	10.7	133
8	5.9	280	2	59.9	4.09	23.4	155	428.0	48.0	63	7.64	79.5
9	8.0	270	2	35.5	3.57	230	182	441.6	74.0	33	5.91	35.6
10	8.0	270	2	36.5	3.60	230	182	427.1	81.0	35	5.53	27.8
11	8.0	270	2	44.5	3.80	281	164	451.7	48.0	44	7.55	88.6
12	8.0	270	2	54.5	4.00	344	149	493.9	42.0	53	11.03	138.3
13	8.0	285	2	35.8	3.58	230	182	360.0	85.0	32	3.93	17.9
14	8.0	285	2	38.4	3.65	230	182	361.1	88.0	31	3.95	16.8
15	8.0	285	2	45.3	3.81	281	164	435.9	60.0	40	7.03	52.8
16	8.0	285	2	53.6	3.98	344	149	468.8	44.0	49	9.94	113.5
17	8.0	300	2	33.4	3.51	230	182	303.4	104.0	30	2.79	8.5
18	8.0	300	2	40.8	3.71	281	164	346.1	74.0	35	4.43	21.9
19	8.0	300	2	49.9	3.91	344	149	392.2	48.0	45	6.96	66.8
20	8.0	300	2	51.7	3.95	344	149	417.6	47.0	49	7.89	78.9
PET-B-1	5.9	280	10	50.0	3.91	190	172	334.0	91.0	180	3.77	13.5
2	5.9	280	5	50.0	3.91	190	172	490.8	59.8	123	8.14	67.4
3	5.9	280	2	50.0	3.91	190	172	461.0	63.0	53	7.18	53.5
4	5.9	280	1	50.0	3.91	190	172	284.0	111.7	25	2.72	6.5
5	5.9	280	0.5	50.0	3.91	190	172	stable				
PP-1	3.7	265	6	19.6	2.98	70.0	273.5	— stable —		—	—	—
2	3.7	265	6	19.9	2.99	71.5	270.6	350	209	74	1.67	2.8
3	3.7	265	6	20.6	3.03	73.5	266.9	472	144	80	3.13	10.7
4	3.7	265	6	22.1	3.10	79.0	257.5	538	104	88	4.37	26.8
5	3.7	265	6	23.1	3.14	82.5	251.9	556	94	94	4.87	35.0
6	3.7	265	6	24.4	3.19	87.1	245.2	560	85	99	5.22	43.4
7	3.7	285	6	21.8	3.08	96.6	232.8	stable				
8	3.7	285	6	24.8	3.21	110.2	218.0	328	139	107	2.26	5.6
9	3.7	285	6	26.0	3.26	115.8	212.6	322	131	114	2.29	6.0

[a] d_0 is the steady-state filament diameter at the take-up computed from the mass throughput G and take-up speed v_w; d_{max} and d_{min} are the measured maximum and minimum filament diameter; L_c is the oscillation period measured along the filament taken up; W_{max} and W_{max}/W_{min} are derived from the d_0, d_{max}, and d_{min} data.

(vi) Limit cycle solutions expressed in $W_{i_w,j}$-versus-j curves, under both Newtonian and power-law viscosity models, have a skewed wave form being steeper on the front of the peak. This fact, overlooked in a previous study,[10] was discovered when N was increased from 100 to 400. The cause and the physical significance of the skewed wave form are not clear to the authors at this moment, although such wave form is a common occurrence in nonlinear vibration (Figs. 1 and 2).

(vii) In Figure 6, W_{max} becomes equal to ψ_w on curve A, signifying that the peak filament diameter at the take-up exceeds the maximum diameter of die swell. That is to say, the filament has thickened in melt spinning, or, still in other words, spinning tension has become negative or compression has taken place at least during part of the draw resonance cycle. This, of course, is not realizable in physical melt spinning. Under such circumstances, spinning tension ≤ 0 becomes an added boundary or restricting condition. Besides, under such near-zero spinning tension, gravity force and surface tension are no more negligible. The region below curve A, therefore, is out of the scope of the present study. This region, the authors believe, represent the dripping liquid droplet-type spinning in which gravity and surface tension play a major role (Fig. 7).

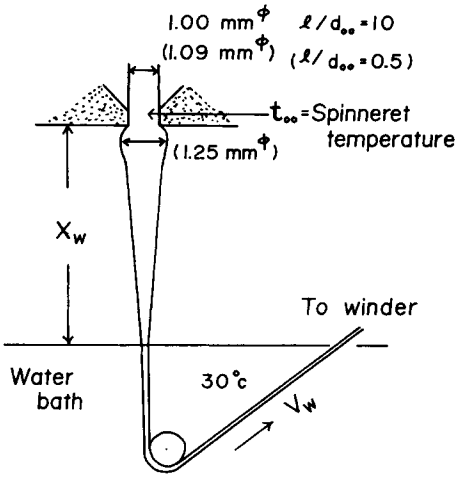

Fig. 9. Schematic of experimental setup. Values in parentheses apply to runs PET-A-1 through 8 and PET-B-1 through 5.

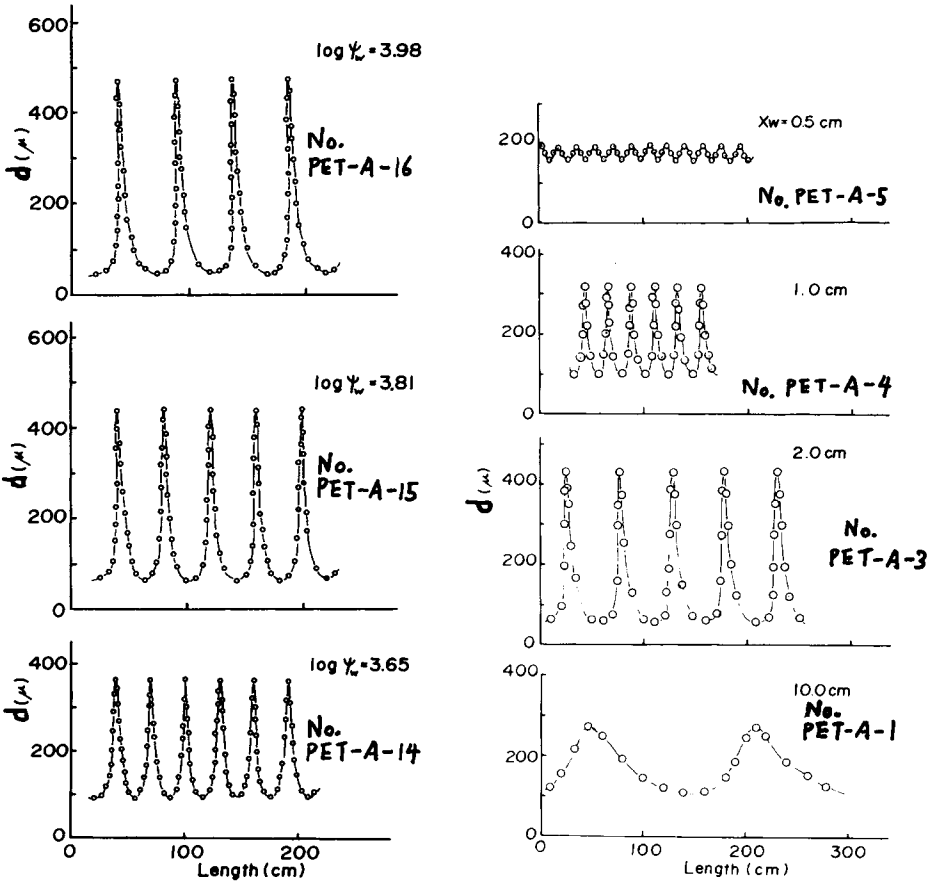

Fig. 10. Experimentally measured wave form of draw resonance for PET in filament diameter-vs.-filament length curves.

Draw Resonance Experiments

Draw resonance experiments were carried out using a conventional fiber-grade PET resin having an IV of 0.563 and designated as PET-A in Table II, a special PET test copolymer containing several weight percent of additive element for an improved dyeability and designated as PET-B and a fiber-grade PP resin. Water quench bath was used in all experiments as shown schematically in Figure 9. No isothermal chamber was used in the spinning of PET-A and PET-B resins since the low Stanton number[9] in these experiments, except in run PET-A-1, ensured[9] approximately isothermal spinning. Isothermal chamber was, however, used in the spinning of PP. Most of the 34 spinning runs listed in Table II resulted in draw resonance. The wave form of draw resonance was observed by measuring the diameter of the fila-

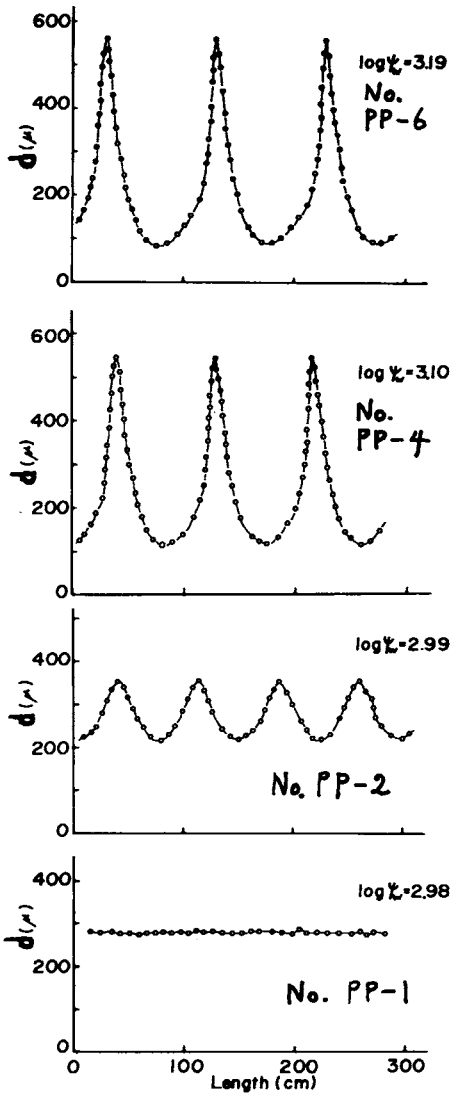

Fig. 11. Experimentally measured wave form of draw resonance for PP.

ment taken up on a winder by means of a high-precision dial gauge. Diameter measurements were made at 2-cm increments near the peak, with the increment increased up to 10-cm as the measurement moved away from the peak. The measured wave forms for 11 of the 34 spinning runs are shown in Figures 10 and 11, respectively, for PET and PP.

The maximum diameters of die swell were measured by photographic means. The maximum diameters were divided into the capillary diameter to obtain the die swell ratios listed below. These ratios are for the spinning conditions listed in Table II. PET-A, 1.13; PET-B, 1.17; PP, 1.21 at 285°C; PP, 1.33 at 265°C.

In computing the steady-state draw down ratio ψ_w listed in Table II, the maximum diameter of die swell was always used rather than the capillary diameter. Otherwise, good agreement between theory and experiment cannot be obtained. Other parameters used in computing ψ_w are the take-up speed

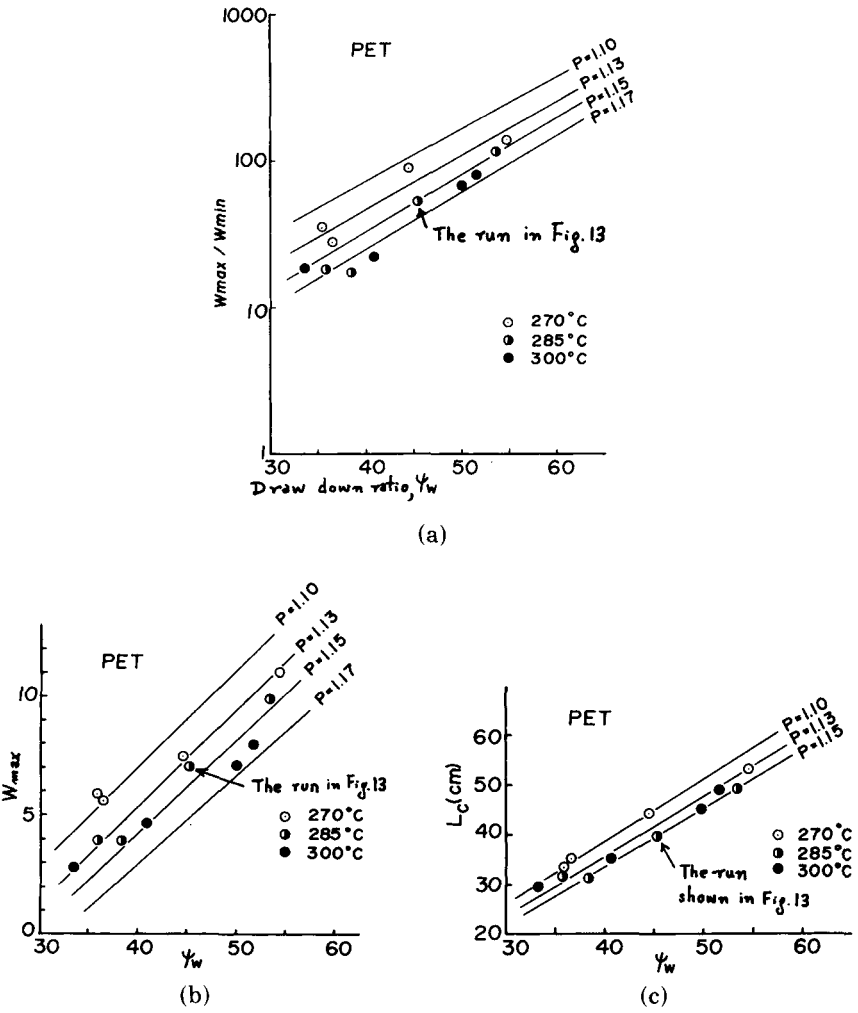

Fig. 12. Comparison of theory and experiment (PET) in the influence of ψ_w on W_{max}/W_{min}, W_{max}, and oscillation period L_c.

v_w, the specific gravity of polymer at the spinning temperatures, and the mass throughput G.

The steady-state filament diameter d_0 in Table II was computed in a like manner.

The W_{max} and W_{max}/W_{min} values in Table II were derived from the measured d_{max} and d_{min} values.

Spinneret capillary dimensions were 1.09 mm diameter and l/d = 0.5 for the first eight runs from PET-A-1 to PET-A-8 and 1.00 mm diameter and l/d = 10 for the rest of the experiments.

The experiments listed in Table II were aimed at seeking the effects of two parameters, draw-down ratio ψ_w and air gap x_w, on the wave form of draw resonance. In the runs PET-A-1 through PET-A-5 and PET-B-1 through PET-B-5, x_w was varied keeping other parameters constant. In the rest of the experiments, ψ_w was varied keeping other conditions unchanged.

DISCUSSION OF EXPERIMENTAL RESULTS

As shown in Figures 12a through 12c, the experimental data for the cross-sectional area ratio W_{max}/W_{min}, the peak cross-sectional area W_{max} (dimensionless), and the oscillation period L_c expressed in the length of filament taken up are plotted against steady-state draw-down ratio ψ_w. These data are for runs PET-A-9 through 20 in Table II. In these spinning runs, the take-up speed v_w (equivalent to ψ_w) and the spinneret temperature t_{00} were varied.

The lines drawn in the above figures are contours of constant p derived from the theoretically computed values listed in Table 1 and summarized in Figures 7 and 8. The contours assign p value to each experimental point.

Figures 12a through 12c show that increasing t_{00} slightly increased the p values. For a given t_{00}, the p value for PET assigned in the above manner was nearly constant over the ψ_w range covered by these experiments and was independent of the three parameters, W_{max}/W_{min}, W_{max}, and L_c, used in the determination of the p value.

This verifies that at least within the scope of these experiments, the power-law model adequately simulated the wave form of draw resonance in PET.

The striking agreement between theory and experiment above can more clearly be demonstrated, as shown in Figure 13, by fitting the experimental

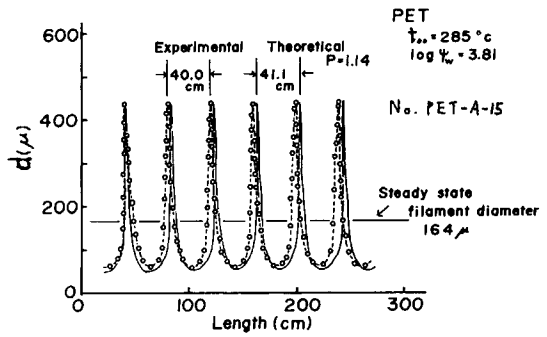

Fig. 13. Excellent agreement of theory and experiment in run PET-A-15.

curve for the run PET-A-15 by the theoretical curve having the ψ_w value given by the experimental condition and the p value of 1.14 which make the theoretical curve agree with experimental curve in W_{max}. In drawing the theoretical curve, time scale was converted from τ^* to filament length L using the relation

$$L = \tau v_w = (\tau v_{00}/x_w)(v_w/v_{00})x_w = (\psi_w x_w)\tau^* \tag{34}$$

where $(\psi_w x_w)$ becomes the conversion factor.

The agreement between theory and experiment was less perfect with PP as shown in Figures 14a through 14c drawn in the same manner as in PET above. The p value remained unchanged for the variation in ψ_w from 19.6 to 24.4 for t_{00} = 265°C, but it differed considerably by the three parameters used in the determination. The p value varied from 0.90 in the L_c diagram to 1.00 in the W_{max}/W_{min} diagram.

It was also noted that the critical draw-down ratio for PP seems to decrease fairly sensitively with increasing t_{00} as far as Figures 14a and 14b show. The extrapolation of this trend seems to agree with the experimental point given by Weinberger[13] as shown in Figure 15, although no conclusion can be drawn

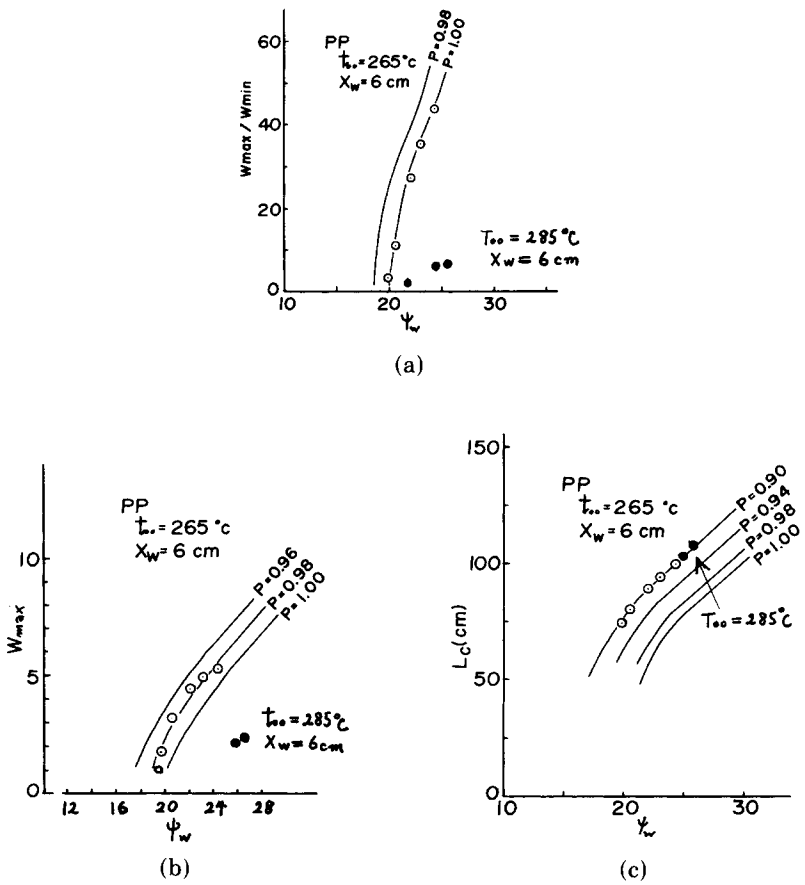

Fig. 14. Comparison of theory and experiment (PP) in the influence of ψ_w on W_{max}/W_{min}, W_{max}, and L_c.

for lack of information on the polymer specifications.

Spinning runs PET-A-1 through 5 and PET-B-1 through 5 were carried out to see the effects of air gap x_w with the results shown in Figures 16a and 16b together with theoretical curves. As discussed previously, W_{max}/W_{min} value should not be affected by x_w under the power law model. For this reason, the theoretical predictions appear as horizontal lines in Figure 16a.

In Figure 16a, the fall-off of the experimental curves on the right-hand end is most likely the effect of the setting-in of the cooling of the filament in air gap. The fall-off starting at a Stanton number of about 0.02 is in general agreement with the discussions made in the previous papers.[9,10] St is in direct proportion to x_w.

The fall-off near the origin, however, is completely unpredicted by the

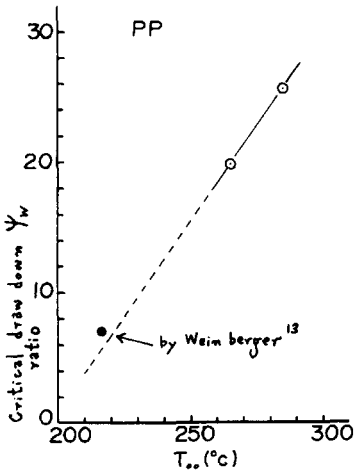

Fig. 15. Effect of spinneret temperature t_{00} on the critical draw-down ratio in the isothermal spinning of PP.

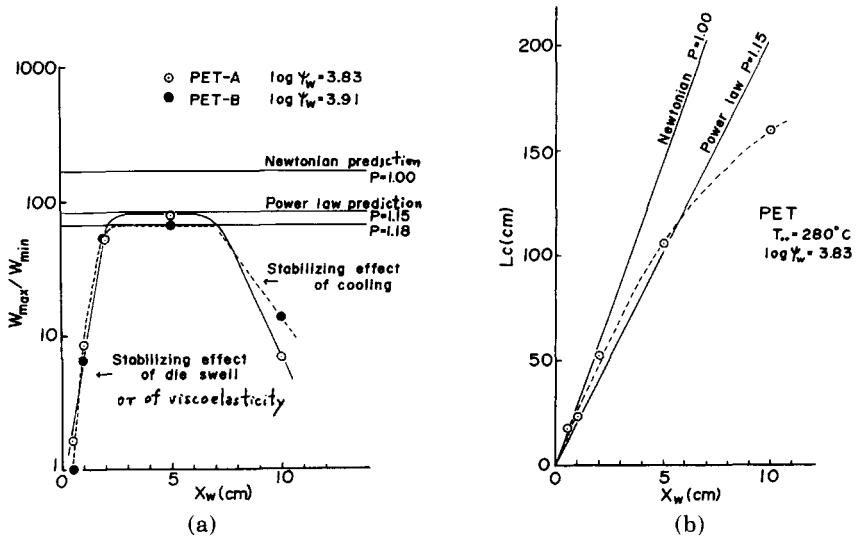

Fig. 16. Influence of air gap x_w on the theoretical and experimental values of W_{max}/W_{min} and L_c. The stabilization at low x_w values is not predicted by the present power law model.

present power law model. In fact, the draw resonance was almost surpressed by narrowing the air gap down to 5 mm. At first, the spring-like elastic nature of the die swell region was suspected to have caused the above stabilizing effect. Later, it was noted that the model proposed by Denn[8] simulating the isothermal spinning of liquids obeying a modified Maxwell viscosity is likely to explain the stabilization of spinning under narrow air gap.

In Denn's above model, unstable spinning can eventually be stabilized by increasing the value of the parameter α, which is defined as

$$\alpha = \frac{v_{00}}{x_w}\theta \tag{35}$$

where θ is the relaxation time of the fluid and v_{00} is the fluid speed at the maximum diameter of die swell; θ may be considered a constant for a given polymer, and v_{00}, too, is a constant unless the metering pump speed is varied. Therefore, decreasing x_w increases α and eventually makes the spinning stable.

In view of the results shown in Figure 16a and the above model by Denn, the power law seems to be adequate under large x_w but the Maxwell model starts to apply as x_w decreases to several milimeters.

As some of the curves in Figure 10 show, the wave form of draw resonance was skewed in the manner as predicted by the theoretical peak shape shown in Figure 2. For comparison with the experimental diameter curves in Figure 10, the $\sqrt{W}$ curve in Figure 2 is more adequate than the W curve.

SIMULATION OF THE SIDE PROFILE OF SPINLINE IN DRAW RESONANCE

When the spinline is observed while in draw resonance, it looks as though water droplets are falling along the spinline at regular time intervals. This peculiarly pulsing side profile was observed and discussed conceptually by Bergonzoni et al.[14] and Zeichner.[7] The limit cycle solutions of the equations of continuity and momentum discussed in the present and the previous[10] studies by the authors made possible, for the first time, the quantitative simulation of the pulsing side profile of the spinline in draw resonance. We now proceed with the simulation.

Motion pictures (16 mm) were taken of pulsing spinline under the spinning conditions below and were compared with theoretical side profiles derived from the corresponding limit cycle solution.

Spinning conditions: polymer, PET; spinneret temperature, t_{00} = 280°C; spinneret hole diameter, d_{00} = 1.6 mm; l/d ratio of spinneret hole, 2.0; take-up speed, v_w 312 m/min (ψ_w = 60); throughput, G = 5.9 g/min; air gap, x_w = 5 cm; water bath temperature, 30°C.

Motion picture conditions: camera, Cine-Kodak Special II; film, 16 mm ASA 40, Fuji Neopan R 40; speed, 64 frames/sec; lens, F 5.6 and 2.8.

The theoretical side profiles shown in Figure 17 were constructed in the following manner: (i) read the $W_{i,j}$ values off the computer printout for the limit cycle solution for p = 1 and ψ_w = 60; (ii) convert i into x using the counterpart[10] of eqs. (4) and (16) for the Newtonian case (p = 1) derived by the

authors previously; (iii) convert j into time τ using eq. (5); (iv) convert $W_{i,j}$ into filament diameter $d(x, \tau)$; and (v) draw 12 side profiles to cover one oscillation period.

Scale factor in the radial direction is arbitrary.

Motion pictures (16 mm) covering one oscillation period are shown in Figure 18. Time spacing of these pictures approximately correspond to that of Figure 17. An excellent agreement may be said to have been obtained between the theoretical and experimental side profiles. The side profile of spinline in draw resonance so far discussed only conceptually[7,14] was successfully simulated.

The data used in constructing the theoretical side profiles yields some ad-

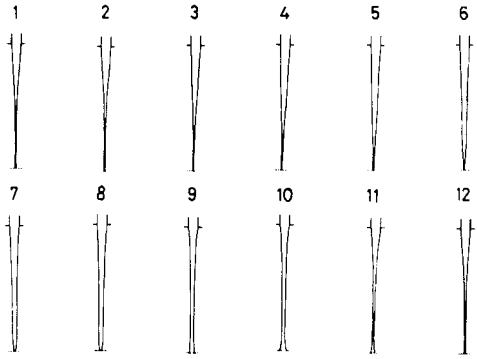

Fig. 17. Theoretically constructed side profiles of spinline in draw resonance; $p = 1$ and $\psi_w = 60$.

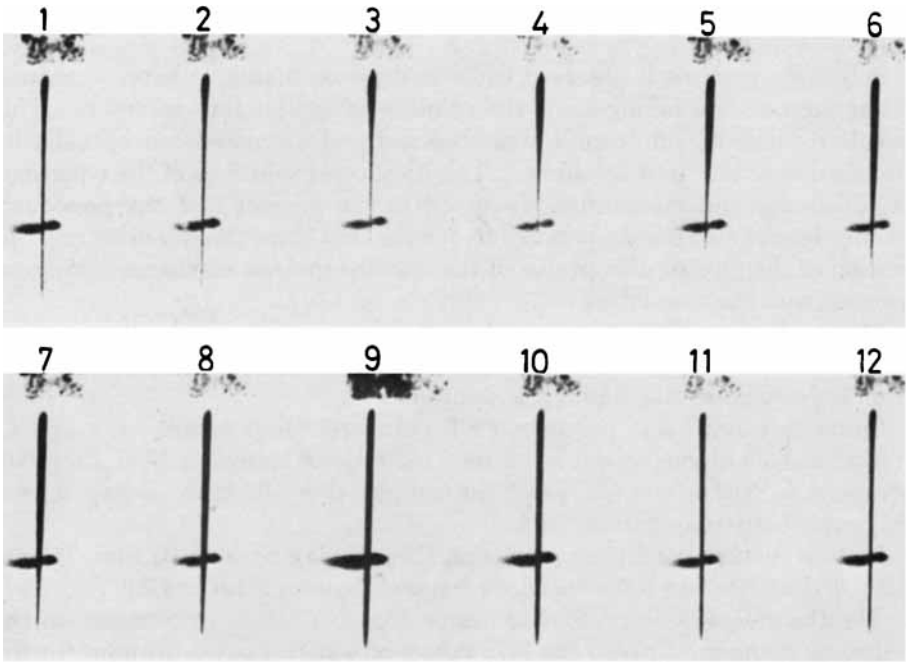

Fig. 18. Motion pictures (16 mm) showing the side profiles of spinline while in draw resonance. The time spacing of pictures approximately correspond to those in Fig. 17.

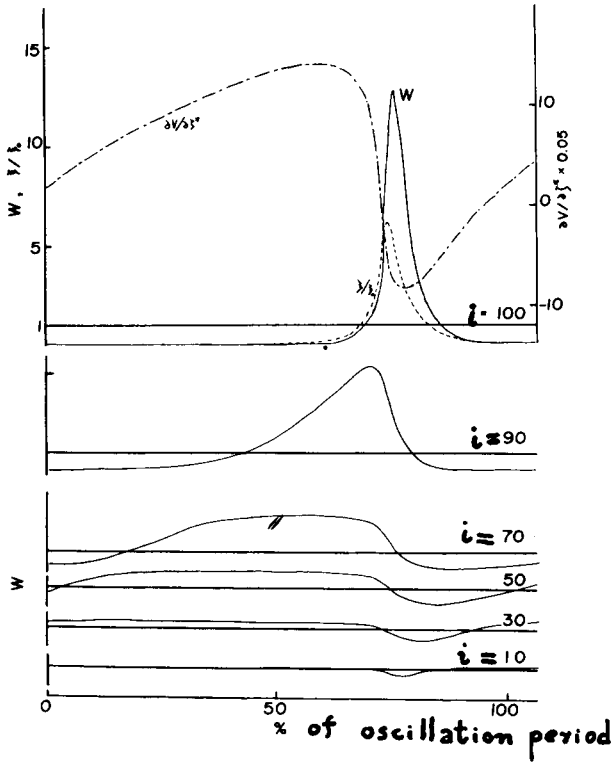

Fig. 19. Time variation of W at different locations i along the spinline. Variation with time of dimensionless spinning tension ξ/ξ_0 and $\partial V/\partial\zeta^*$ at the take-up point.

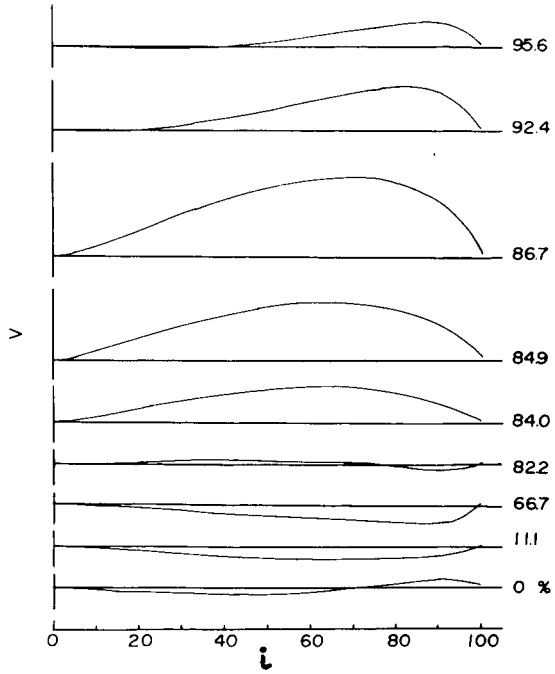

Fig. 20. Variation of V with time at different locations i along the spinline.

ditional information. Shown in Figure 19 are $W_{i,j}$ values plotted against time for different positions along the spinline. Also plotted in Figure 19 are time variation of spinning tension and the $\partial V/\partial\zeta^*$ values at the take-up point. Spinning tension variation is similar in wave form to W but slightly ahead in phase. $\partial V/\partial\zeta^*$ is not a direct measure of the shear rate $\partial v/\partial x$. The two quantities are related by eq. (36) below:

$$\partial v/\partial x_{(x=x_w)} = \frac{v_{00}\psi_w{}^q}{x_w}\left[\frac{\zeta^* + \omega}{\omega}\frac{\partial V}{\partial\zeta^*} - \frac{V}{q\omega}\right]. \tag{36}$$

Shown in Figure 20 are dimensionless velocity profiles along the spinline at different phases in the draw resonance cycle.

A BRIEF DISCUSSION ON THE RELATION BETWEEN THE STABILITY OF MELT SPINNING AND THE SPINNABILITY OF FLUIDS

The present theoretical analysis, which showed good agreement with experiments, provides information as to under what conditions the melt spinning becomes unstable, and, once unstable, to what extent the filament thins down in draw resonance. The present theory, however, tells little about the spinnability of the polymer since the breakage of the filament is not covered.

While the filament has to thin down before it can break, draw resonance is not the only way to thin down the filament. In fact, the simple stretching of a cylindrical fluid element or increasing the draw-down ratio in a stable melt spinning is equivalent in thin-down effect. Besides, spinning instability or draw resonance is a phenomenon that takes place only under very special conditions so that it is hardly related to the spinnability problem which is concerned with a much wider range of conditions.

Therefore, the spinnability of fluids and the stability of melt spinning are considered to be two independent problems having no direct equivalence. The spinnability problem should better be discussed under the much simpler geometry of cylinder stretching.

CONCLUSIONS

The equations of continuity and momentum with the power-law viscosity model were solved for nonlinear limit cycle solutions using different values of the power-law exponent p and steady-state draw-down ratio ψ_w; p and ψ_w are the only parameters that affect the normalized wave form of the limit cycle solutions.

Water-quenched melt spinning of PET and PP was carried out under 34 different spinning conditions to measure the wave form of draw resonance. The following are the conclusions drawn from the computations and experiments:

1. The contours of constant amplitude of limit cycle, including the neutral stability curve, were found to be approximately straight lines in the p-versus-log ψ_w plane.

2. The theoretical wave form based on the power-law viscosity model showed excellent agreement with PET experiments in that the superposition

of the theoretical values of amplitude W_{max}, W_{max}/W_{min}, and oscillation period τ_c* on the respective experimental values gave nearly identical p values and that the p value was approximately independent of ψ_w over the range covered by the experiments. A nearly perfect fit of the theoretical and experimental wave form was also obtained. Agreement of theory and experiment was less perfect with PP.

3. Decreasing the air gap x_w to about 15 mm or below tended to surpress the draw resonance. This fact, totally unpredicted by the present power law model, seems to be explained by the modified Maxwell model proposed by Denn.[8]

4. The computed limit cycle solutions were skewed in the form of the wave peaks. Similar skewed wave form was observed experimentally.

5. Motion pictures (16 mm) of the side profiles of spinline in draw resonance agreed well with the theoretical side profiles.

6. It was discussed that the stability of melt spinning has no direct equivalence to the spinnability of fluids.

In summary, a nearly perfect simulation of the phenomenon of draw resonance was obtained, except under very narrow air gap, using the power-law viscosity model.

The authors wish to express their sincerest thanks to Dr. T. K. Matsumoto who encouraged the conduct of the present study; to Mr. H. Yasuda, Mr. T. Aihara, and Mr. Y. Matsui, all of Toyobo Co., Ltd., for their cooperation in experiments; and to Professor M. M. Denn of the University of Delaware for sending his papers on the stability of the spinning of Maxwell-type liquids prior to publication.

References

1. J. C. Miller, *SPE Trans.*, **3,** 134 (1963).
2. S. Kase, T. Matsuo, and Y. Yoshimoto, *Seni Kikai Gakkaishi* (*J. Japan Tex. Mach. Soc.*), **19,** T63 (1966).
3. J. R. A. Pearson and M. A. Matovich, *Ind. Eng. Chem., Fundam.*, **8,** 605 (1969).
4. D. Gelder, *Ind. Eng. Chem., Fundam.*, **10,** 534 (1971).
5. Y. T. Shah and J. R. A. Pearson, *Ind. Eng. Chem., Fundam.*, **11,** 145 (1972).
6. Y. T. Shah and J. R. A. Pearson, *Polym. Eng. Sci.*, **12,** 219 (1972).
7. G. R. Zeichner, Master of Chem. Eng. Thesis, University of Delaware, 1973.
8. M. M. Denn, *Stability of Reaction and Transport Processes,* Prentice-Hall, Englewood Cliffs, N.J., 1975, pp. 160–164.
9. S. Kase, *J. Appl. Polym. Sci.*, **18,** 3279 (1974).
10. H. Ishihara and S. Kase, *J. Appl. Polym. Sci.*, **19,** 557 (1975).
11. R. J. Fisher and M. M. Denn, *Chem. Eng. Sci.*, **30,** 1129 (1975).
12. S. Kase and T. Matsuo, *J. Polym. Sci. A,* **3,** 2541 (1965).
13. C. F. Weinberger, personal communication 1975.
14. A. Bergonzoni and J. DiCresce, *Polym. Eng. Sci.*, **6,** 45 (1966).

Received January 16, 1975
Revised May 15, 1975